Mathematical Modeling and Numerical Analysis of SPIM Drive Using Modified SVPWM Technique

Vishal Rathore† and **Krishna Bihari Yadav**, Non-members

ABSTRACT

This paper presents a modified space-vector pulse width modulation (SVPWM) technique for a five-level inverter that provides complete control over the multiple space-vector voltages of a six-phase inverter. This technique involves splitting six phases into two three-phase five-level inverters connected in parallel. A six-phase induction motor (SPIM) drive with a distributed neutral is considered as the load. This paper also presents a comparative analysis between the proposed and conventional SVPWM inverter-fed SPIM drives. To investigate the analytical developments and voltage limits, MATLAB/Simulink environment was used in this study. A prototype was developed in the laboratory for analyzing the harmonic components of the phase voltages and currents. The efficacy of the proposed technique was validated by means of comprehensive experiments, and the results discussed herein.

Keywords: Six-Phase Induction Motor Drive, SPIM Drive, Five-Level Inverter, Space-Vector Pulse Width Modulation, SVPWM, Harmonic Analysis

1. INTRODUCTION

In recent times, high-performance induction motor drives have been extensively utilized in various high-power applications owing to their rugged construction and low maintenance requirement. Generally, high-power electrical drives require converters with high-frequency semiconductor switches, which are either unavailable in the market or expensive. This drawback is overcome by employing a multi-phase converter and multi-phase drives, which can divide the power among the semiconductor devices. Their utilization reduces the current in each phase without any change in per-phase voltage. In addition, multi-phase induction motor drives have various potential advantages over their three-phase counterparts. These advantages include increasing power in the stator frame, expanding the frequency of torque pulsations, decreasing the amplitude of pulsating torque, and reducing DC-link current harmonics. Moreover, owing to their expendable structure, they have high reliability. Therefore, the multi-phase voltage source inverter and multi-phase induction motor drive effectively obtain high power ratings for drive applications [1, 2].

A multi-phase machine can be set up with any number of phases from the traditional three-phase machine by spatially shifting the stator winding by δ electrical degrees. However, the best performance is obtained in the case of six phases [3]. Therefore, a six-phase induction motor (SPIM) in an asymmetrical configuration is the most frequently used for high power applications. It is constructed from a conventional machine by rearranging the 60-degree phase displacement of a stator winding into two, spanning $\delta = 30$ electrical degrees, whereas the cage type rotor winding is used. As a result, the current rating of the semiconductor switches used in the five-level inverter are halved for the same power rating.

In this study, an efficient SPIM was modeled using space-vector transformation. Its behavior was studied by two independent space vectors, q_1-d_1 and q_5-d_5, rotating arbitrarily in the q-d reference frame, and a suitable pulse width modulation technique adopted to control the multiple voltages of the space vectors. An algorithm was developed to control the different voltages of the two space vectors based on the space-vector model introduced in [4]. Modified versions of the same modulation scheme are presented in [5–7]. Though they are capable of reducing the voltage and current harmonics, these schemes are fairly complex. Unlike the above methods, a simple decomposition of the three phases using a single vector moving in the q-d frame is presented in [8–10]. The space-vector pulse width modulation (SVPWM) technique proposed in this paper allows complete control of two space vectors applied to two five-level inverters connected in parallel, the output of which is fed into a SPIM drive. Moreover, to validate its superlative performance, the proposed technique was compared with the conventionally designed SVPWM technique. Finally, a prototype model was developed in the laboratory, based on mathematical modeling. The values of voltage, current, and harmonics were recorded using the power analyzer scope Yokogawa DL750, and the effectiveness of the proposed technique verified using the FLUKE analyzer.

Manuscript received on August 21, 2021; revised on October 4, 2021; accepted on October 24, 2021. This paper was recommended by Associate Editor Yuttana Kumsuwan.

The authors are with the Department of Electrical Engineering, National Institute of Technology Jamshedpur, Jharkhand, India.

†Corresponding author: vishalrathore01@gmail.com

Digital Object Identifier: 10.37936/ecti-eec.2022202.246877

2. SPACE VECTOR TRANSFORMATION OF FOR SIX-PHASE INVERTER

The space vector can be generally expressed by transforming an asymmetric six-phase system as in [11]:

$$\bar{s}_v = \frac{1}{3}\left[s_1 + s_2 e^{j\frac{v\pi}{6}} + s_3 e^{j\frac{4v\pi}{6}} + s_4 e^{j\frac{5v\pi}{6}} + s_5 e^{j\frac{8v\pi}{6}} + s_6 e^{j\frac{9v\pi}{6}}\right] \quad (1)$$

where $v = 1, 3, 5$, thus Eq. (1) can be transformed to a set of three space vectors as:

$$\bar{s}_1 = \frac{1}{3}\left[s_1 + s_2 e^{j\frac{\pi}{6}} + s_3 e^{j\frac{4\pi}{6}} + s_4 e^{j\frac{5\pi}{6}} + s_5 e^{j\frac{8\pi}{6}} + s_6 e^{j\frac{9\pi}{6}}\right] \quad (2)$$

$$\bar{s}_3 = \frac{1}{3}\left[(s_1 + s_3 + s_5) + (s_2 + s_4 + s_6)\right] \quad (3)$$

$$\bar{s}_5 = \frac{1}{3}\left[s_1 + s_2 e^{j\frac{5\pi}{6}} + s_3 e^{j\frac{8\pi}{6}} + s_4 e^{j\frac{\pi}{6}} + s_5 e^{j\frac{4\pi}{6}} + s_6 e^{j\frac{9\pi}{6}}\right] \quad (4)$$

It should be noted that the machine has six phases, such that the expression for the vector $\bar{s}_3$ is non-singular. As 3 is a factor of 6, which is not a prime number, by taking inverse transformation, the new sets of six space vectors are reformulated as:

$$s_1 = \bar{s}_1 + \bar{s}_3 + \bar{s}_5^* \quad (5)$$

$$s_2 = \left(\bar{s}_1 - \bar{s}_5^*\right) \cdot e^{j\frac{\pi}{6}} + j \cdot \bar{s}_3 \quad (6)$$

$$s_3 = \left(\bar{s}_1 + \bar{s}_5^*\right) \cdot e^{j\frac{4\pi}{6}} + \bar{s}_3 \quad (7)$$

$$s_4 = \left(\bar{s}_1 - \bar{s}_5^*\right) \cdot e^{j\frac{5\pi}{6}} + j \cdot \bar{s}_3 \quad (8)$$

$$s_5 = \left(\bar{s}_1 + \bar{s}_5^*\right) \cdot e^{j\frac{8\pi}{6}} + \bar{s}_3 \quad (9)$$

$$s_6 = \left(\bar{s}_1 - \bar{s}_5^*\right) \cdot e^{j\frac{9\pi}{6}} + j \cdot \bar{s}_3 \quad (10)$$

where '*' and '·' denote the complex conjugate and scalar product, respectively. The space vectors s_1, s_3, and s_5 lie in q_1-d_1, q_3-d_3, and q_5-d_5 planes, respectively.

The six space vectors are decomposed into two sets, and one set has odd vectors $s_{a1} = s_1$, $s_{b1} = s_3$, $s_{c1} = s_5$ and another has even vectors $s_{a2} = s_2$, $s_{b2} = s_4$, $s_{c2} = s_6$. The sub-system vectors $\bar{s}_{abc,1}$, $\bar{s}_{abc,2}$ and their zero-sequence components s_{o1}, s_{o2} are expressed in the form of multiple space vectors by the sets of equations as:

$$\bar{s}_{abc,1} = \frac{2}{3}\left[s_{a1} + s_{b1} e^{j\frac{4\pi}{6}} + s_{c1} e^{j\frac{8\pi}{6}}\right] \quad (11)$$

$$\bar{s}_{abc,2} = \frac{2}{3}\left[s_{a2} + s_{b2} e^{j\frac{4\pi}{6}} + s_{c2} e^{j\frac{8\pi}{6}}\right] \quad (12)$$

$$s_{o1} = \frac{1}{3}\left[s_{a1} + s_{b1} + s_{c1}\right] \quad (13)$$

$$s_{o2} = \frac{1}{3}\left[s_{a2} + s_{b2} + s_{c2}\right] \quad (14)$$

$$\bar{s}_{abc,1} = \left[\bar{s}_1 + \bar{s}_5^*\right] \quad (15)$$

$$\bar{s}_{abc,2} = \left[\bar{s}_1 - \bar{s}_5^*\right] e^{-j\frac{\pi}{6}} \quad (16)$$

$$s_{o1} = \bar{s}_3 \quad (17)$$

$$s_{o2} = j \cdot \bar{s}_3 \quad (18)$$

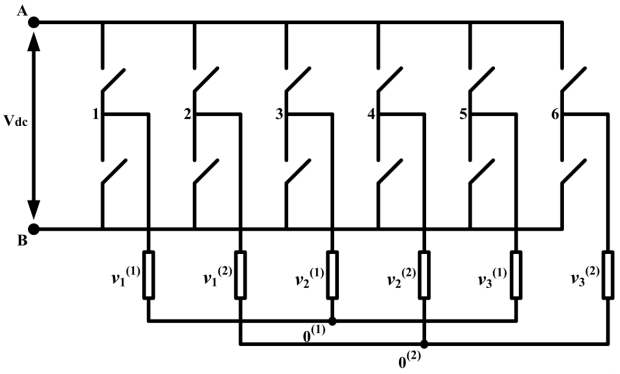

***Fig. 1**: Five-level six-phase inverter fed SPIM with an isolated neutral.*

3. SVPWM INVERTER-BASED SPIM DRIVE

The proposed modified SVPWM technique for a five-level six-phase inverter feeding a SPIM with isolated neutral points $0^{(1)}$ and $0^{(2)}$ is illustrated in Fig. 1. The six voltages can be represented as the combination of two three-phase voltages. Likewise, it can be seen that the six-phase inverter behaves as two three-phase inverters supplied by a common DC voltage. The six output voltages (v_{a1}, v_{b1}, v_{c1}, v_{a2}, v_{b2}, v_{c2}) of the inverter are transformed to two multiple space vectors [12] as:

$$\bar{v}_1 = \frac{1}{3} v_{dc}\left[v_{a1} + v_{a2} e^{j\frac{\pi}{6}} + v_{b1} e^{j\frac{4\pi}{6}} + v_{b2} e^{j\frac{5\pi}{6}} + v_{c1} e^{j\frac{8\pi}{6}} + v_{c2} e^{j\frac{9\pi}{6}}\right] \quad (19)$$

$$\bar{v}_5 = \frac{1}{3} v_{dc}\left[v_{a1} + v_{a2} e^{j\frac{5\pi}{6}} + v_{b1} e^{j\frac{8\pi}{6}} + v_{b2} e^{j\frac{\pi}{6}} + v_{c1} e^{j\frac{4\pi}{6}} + v_{c2} e^{j\frac{9\pi}{6}}\right] \quad (20)$$

Four null space vectors correspond to 64 possible switching states in $q1$-$d1$ and $q5$-$d5$ reference sub-space (000000, 111111, 101010, 010101). The remaining 60 vectors are active and categorized as the largest, second-largest, and third-largest. Among these, 12 vectors are redundant and consider the third-largest vector obtained by combining two switching states. The projection of vectors in $q1$-$d1$ and q_5-d_5 sub-space is depicted in Figs. 2(a) and 2(b), respectively. In a conventional six-phase induction motor, there is only one neutral, but in this particular case, the divided neutral is considered, so when the system is connected to the load, it results in $v_{01} = v_{02} = 0$ and $v_3 = 0$. The remaining vectors are formulated as

$$\bar{v}_{abc,1} = \frac{2}{3} v_{dc}\left[v_{a1} + v_{b1} e^{j\frac{\pi}{2}} + v_{c1} e^{j\pi}\right] \quad (21)$$

$$\bar{v}_{abc,2} = \frac{2}{3} v_{dc}\left[v_{a2} + v_{b2} e^{j\frac{\pi}{2}} + v_{c2} e^{j\pi}\right] \quad (22)$$

The space vectors $\bar{v}_{abc,1}$ and $\bar{v}_{abc,2}$ in terms of output voltage in q_1-d_1 and q_5-d_5 sub-space are illustrated in Fig. 3. The reference voltage vector of six-phase SVPWM

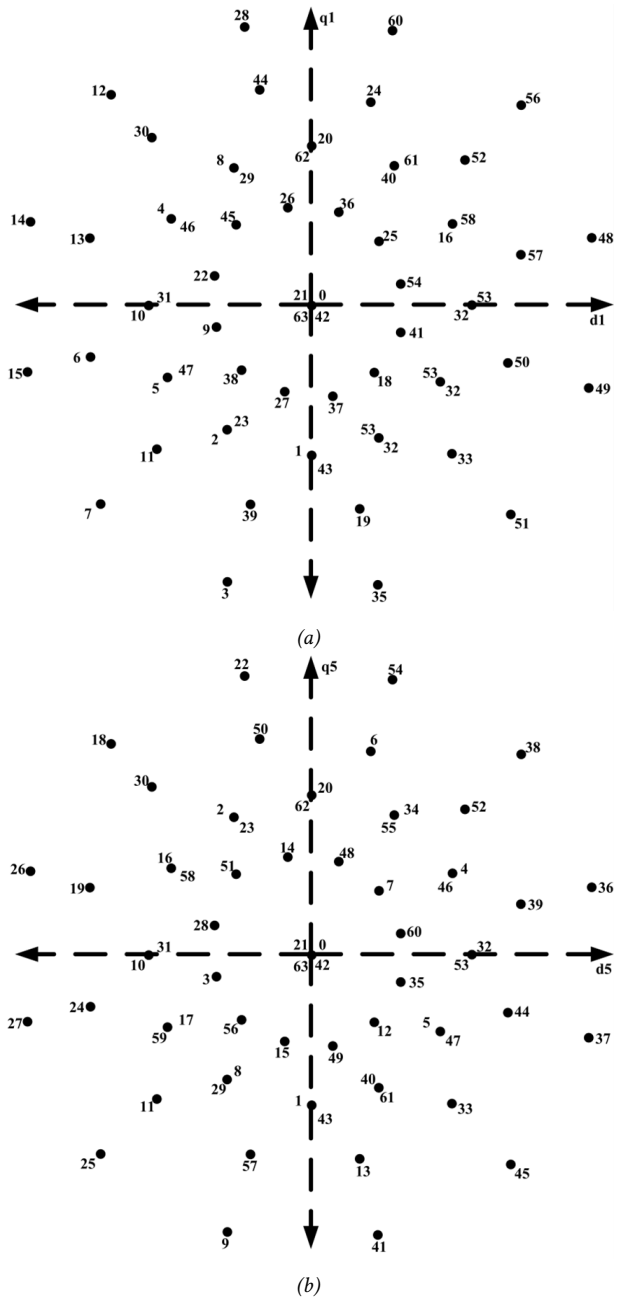

***Fig. 2**: Mapping of space vectors on (a) q_1-d_1 sub-space and (b) q_5-d_5 sub-space.*

is used to determine the reference space vector of two three-phase as:

$$\overline{v}_{r1} = \left[\overline{v}_{1r} + \overline{v}_r^*\right] \tag{23}$$

$$\overline{v}_{r2} = \left[\overline{v}_{2r} - \overline{v}_r^*\right] e^{-j\frac{\pi}{6}} \tag{24}$$

The duty cycles $D_{1,1}$, $D_{1,2}$, $D_{2,1}$, and $D_{2,2}$ corresponding to the voltage $\overline{v}_{1,1}$, $\overline{v}_{1,2}$, $\overline{v}_{2,1}$, and $\overline{v}_{2,2}$, respectively are given by the following sets of equations:

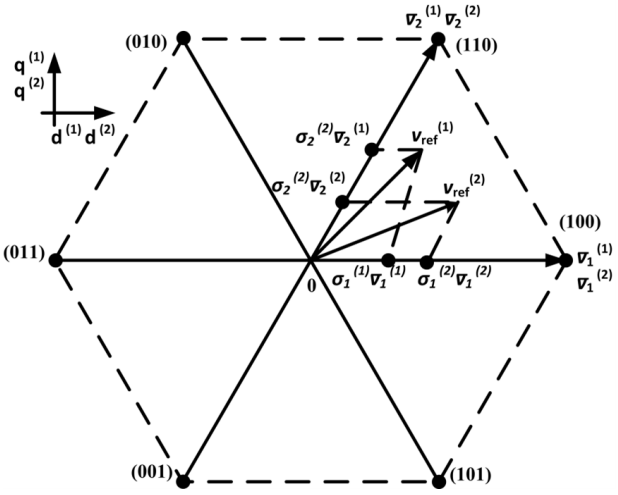

***Fig. 3**: Projection of voltage space vectors on q-d sub-space.*

$$D_{1,1} = \frac{\overline{v}_{1r,1} \cdot j\overline{v}_{2,1}}{\overline{v}_{1,1} \cdot j\overline{v}_{1,1}} \tag{25}$$

$$D_{1,2} = \frac{\overline{v}_{1r,1} \cdot j\overline{v}_{1,1}}{\overline{v}_{2,1} \cdot j\overline{v}_{2,1}} \tag{26}$$

$$D_{2,1} = \frac{\overline{v}_{1r,1} \cdot j\overline{v}_{1,1}}{\overline{v}_{2,1} \cdot j\overline{v}_{2,1}} \tag{27}$$

$$D_{2,2} = \frac{\overline{v}_{1r,2} \cdot j\overline{v}_{1,2}}{\overline{v}_{2,2} \cdot j\overline{v}_{2,2}} \tag{28}$$

The null vectors (000) and (111) duty cycles $D_{0,1}$, $D_{0,2}$, $D_{3,1}$, and $D_{3,2}$ are used to complete the switching period. Moreover, these null vectors provide an additional two degrees of freedom to control the switching frequency and reduce the current ripple.

$$D_{0,1} + D_{3,1} = 1 - \left(D_{1,1} + D_{2,1}\right) \tag{29}$$

$$D_{0,2} + D_{3,2} = 1 - \left(D_{1,2} + D_{2,2}\right) \tag{30}$$

The switching frequency can be controlled by utilizing two modes of operation, namely, continuous mode, in which the duty cycle of a null vector is not equal to zero, and the discontinuous mode, in which the respective duty cycles of all the null vectors are zero.

4. CONVENTIONAL SVPWM INVERTER-BASED SPIM DRIVE

The conventional SVPWM technique for the SPIM drive is similar to that of a three-phase induction motor drive. This technique uses the null vector and two adjacent active vectors to synthesize the reference voltage vector. The *q-d* sub-space is equally distributed into 12 sectors, each of 30-degrees as shown in Fig. 4, and the presence of reference voltage vectors decides the sectors' position. The largest vector lies on the outermost 12-side polygon. If the reference vector is present in

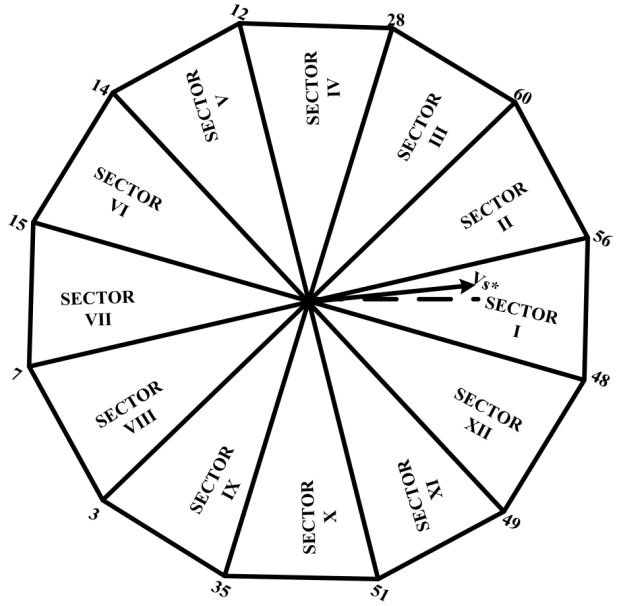

***Fig. 4**: Selected switching modes of conventional SVPWM.*

Sector-I, then the vectors $\mathbf{V_{48}}$ and $\mathbf{V_{49}}$ are utilized, and the switching time of the corresponding space vector can be calculated as:

$$\tau = 2m_a\tau_s \sin\left(\frac{\pi}{6} - \theta\right) \tag{31}$$

$$\tau = 2m_a\tau_s \sin\theta \tag{32}$$

$$\tau_0 = \tau_s - \tau_1 - \tau_2 \tag{33}$$

where m_a is the modulation index; the maximum value of m_a is 0.9679 in accordance with the phase voltage, whereas in the case of three-phase SVPWM, the phase voltage is lower due to the addition of the harmonic components in the output waveform.

5. SPIM MODELING

The performance of the proposed asymmetrical SPIM model is analyzed by transforming the pair of three-phase equations in a *q-d* reference frame. The equivalent circuit of SPIM [13] in *q-d* sub-space is depicted in Fig. 5, and equations can be written as:

$$v_d = \frac{1}{3}\left[\sum_{k=1}^{6} v_k \cos\left(\theta - \frac{(k-1)\,\pi}{6}\right)\right] \tag{34}$$

$$v_q = \frac{1}{3}\left[\sum_{k=1}^{6} v_k \cos\left(\theta - \frac{(k-1)\,\pi}{6}\right)\right] \tag{35}$$

The *d-q* axis flux and current component of stator and rotor can be expressed as:

***Table 1**: Parameters of SPIM drive.*

Power (P)	1 HP
Voltage (V)	220 V
Frequency (f)	50 Hz
Speed (ω_r)	1500 rpm
Current (i)	1.8 A
Stator Resistance (R_s)	4.1 Ω
Rotor Resistance (R_r)	4.1 Ω
Mutual inductance (L_m)	782.7 mH
Stator and rotor inductance (L_s, L_r)	808.1 mH
Moment of inertia (J)	0.0088 kg·m^2

$$\Psi_{ds} = \frac{1}{s}\left[-\omega_e\Psi_{qs} - R_s i_{ds} + v_{ds}\right] \tag{36}$$

$$i_{ds} = \frac{1}{L_s}\left[\Psi_{ds} - L_m i_{dr}\right] \tag{37}$$

$$\Psi_{dr} = \frac{1}{s}\left[(\omega_e - \omega_r)\,\Psi_{qr} - R_r i_{dr}\right] \tag{38}$$

$$i_{dr} = \frac{1}{L_r}\left[\Psi_{qr} - L_m i_{ds}\right] \tag{39}$$

$$\Psi_{qs} = \frac{1}{s}\left[-\omega_e\Psi_{ds} - R_s i_{qs} + v_{qs}\right] \tag{40}$$

$$i_{qs} = \frac{1}{L_s}\left[\Psi_{qs} - L_m i_{qr}\right] \tag{41}$$

$$\Psi_{qr} = \frac{1}{s}\left[(\omega_r - \omega_e)\,\Psi_{dr} - R_r i_{qr}\right] \tag{42}$$

$$i_{qr} = \frac{1}{L_r}\left[\Psi_{qr} - L_m i_{qs}\right] \tag{43}$$

The torque and speed can be expressed as follows:

$$T_e = \frac{3P}{2}\left[\Psi_{ds} i_{qs} - \Psi_{qs} i_{ds}\right] \tag{44}$$

$$\omega_r = \frac{P}{2s}\left[\frac{1}{J}\left(T_e - T_L - \Delta\frac{2}{P}\omega_r\right)\right] \tag{45}$$

where ω_r is the angular speed, ω_e is the arbitrary reference speed, P is the pole pair, subscripts s and r refer to stator and rotor, respectively, L_m is the mutual inductance, J is the moment of inertia, and T_e and T_L are the electric and load torque, respectively.

6. SIMULATION RESULTS AND ANALYSIS

The proposed modified SVPWM based five-level inverter-fed SPIM drive was first modeled in the MATLAB/Simulink environment, as illustrated in Fig. 6. Numerical simulations were utilized to test the behavior of the system. The model was simulated numerically by using the parameters shown in Table 1. For simulation purposes, the value of DC bus voltage (V_{dc}) was assumed to be 200 V, and the reference speed of the machine taken as 1470 rpm.

For the null configuration, the following relationships between the duty cycles were assumed: $D_{0,1} = D_{3,1}$ and

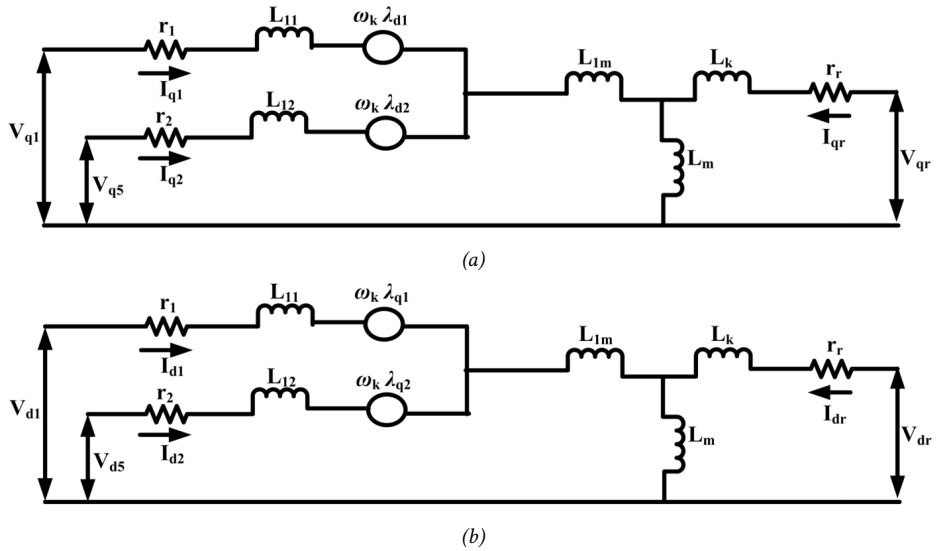

***Fig. 5**: Equivalent circuit of SPIM (a) q-axis and (b) d-axis.*

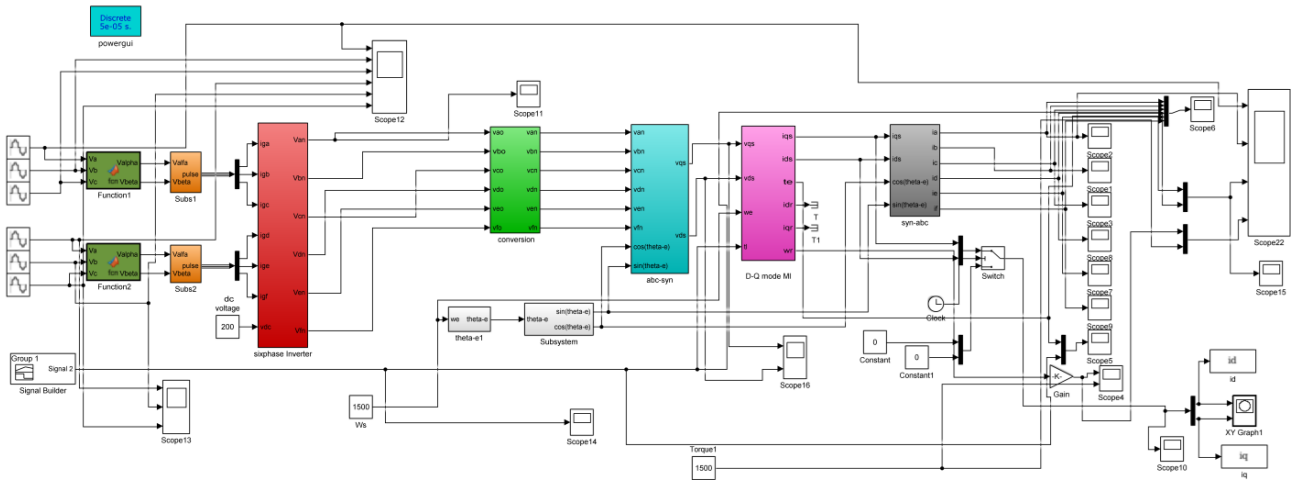

***Fig. 6**: Mathematical model of the proposed SPIM drive.*

$D_{0,2} = D_{3,2}$ at a switching period ($\tau = 200\,\mu$s), while the resultant space-vector scheme is the same as that of the conventional SVPWM for the two three-phase inverters.

To verify the effectiveness of the system, the proposed model was analyzed using two cases. In the first case, the simulation test was performed under balance conditions by supplying purely sinusoidal stator reference voltage of magnitude $V_{1ref} = 150$ V at a frequency of 50 Hz, and the reference voltage V_{5ref} set to 0 V. Fig. 7 shows a five-level line-to-neutral inverter output representing the stator phase voltage (V_{s1}) with its harmonic profile. It is evident from the output that the phase voltage contains only the fundamental component and the remaining harmonic components are zero. Fig. 8 illustrates the variation of six-phase currents under variable-load conditions. Next, harmonic analysis was performed under the steady-state condition on a per-phase basis for the stator current (I_{s1}), as depicted in Fig. 9. The current waveform is clearly shown as being sinusoidal, and except for the fundamental component, other harmonics components are almost negligible or zero. Fig. 10 depicts the variation of the stator currents i_{s1} and i_{s5} in the q_1-d_1 reference plane.

In similarity to the first case, in the second case, the simulation test was performed under balanced conditions. However, the only difference was that a non-sinusoidal supply fed a purely sinusoidal supply machine by introducing the fifth harmonic component in the reference voltage waveform with a voltage magnitude 250 V at a frequency of 250 Hz. Fig. 11 shows the five-level line-to-neutral voltage of the inverter (stator phase voltage). It can be observed that the waveform of the phase voltage is the same as that of the previous case, but the harmonic analysis reveals that it clearly contains fundamental and fifth harmonic components. Fig. 12 depicts the variation of stator currents under change of load conditions. Similar to the first case, the analysis of the current waveform was performed on a

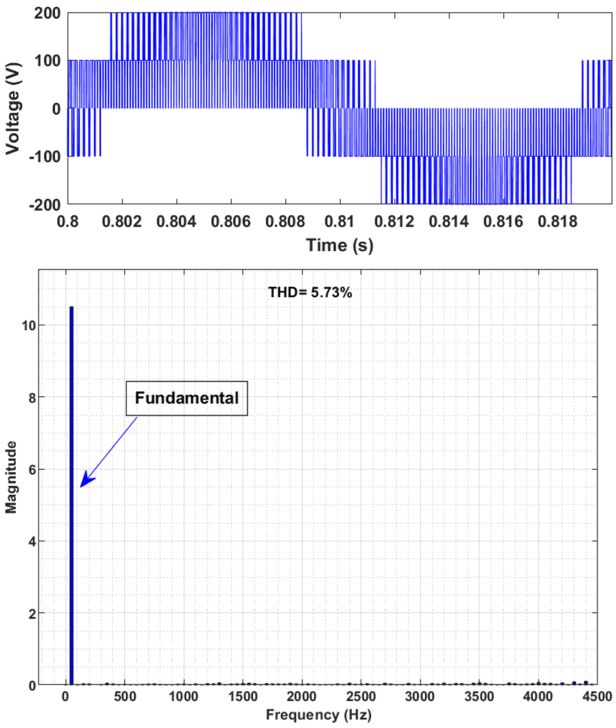

***Fig. 7**: Five-level stator phase voltage with a fundamental component.*

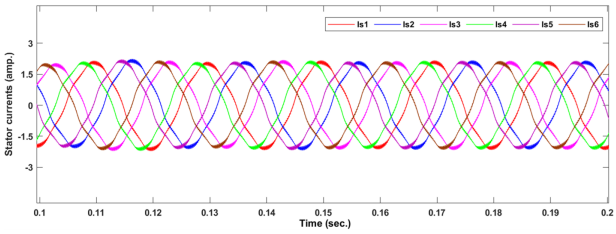

***Fig. 8**: Variation of stator currents in q_1-d_1 sub-space.*

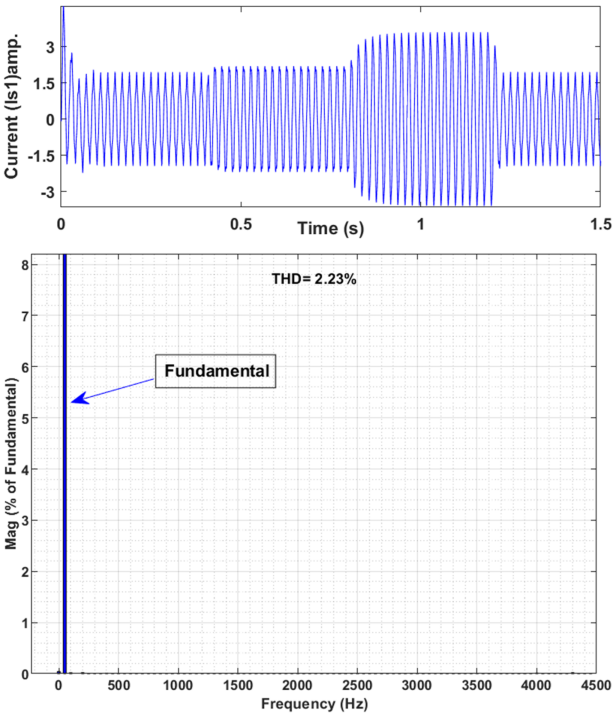

***Fig. 9**: Stator current I_{s1} with harmonic content in q_1-d_1 sub-space.*

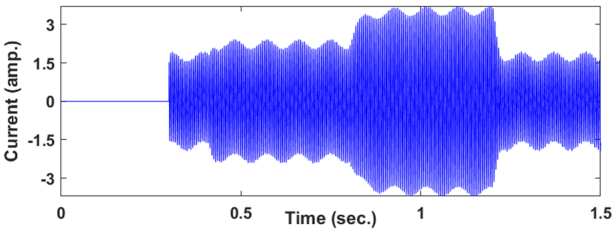

***Fig. 10**: Variation of stator currents I_{s1} and I_{s5} in q_1-d_1 sub-space.*

per-phase basis by considering the steady-state condition depicted in Fig. 13. It is clear from the results that the stator current (I_{s1}) only contains fundamental and fifth harmonic components. Fig. 14 shows the variation of the stator currents i_{s1} and i_{s5} in the q_5-d_5 reference plane. In both the cases, under no-load conditions, the SPIM drive starts normally at the instant $t_1 = 0.4$ s and a load torque of 12 Nm, while at $t_2 = 0.8$ s, a load torque of 18 Nm is applied to the motor (see Fig. 15) as a result of which the machine draws more current and the speed of the motor slightly reduces. As soon as the value of load torque becomes zero, the SPIM reverts to the reference speed.

The simulation results of the two cases verify the effective implementation of the proposed SVPWM scheme. The results of this study are further substantiated in the next section through experimental validation.

7. HARDWARE IMPLEMENTATION

The prototype system comprises high-rating semiconductor switches, while the insulated-gate bipolar transistor IGBT (6W30NC120HD) for the five-level inverter is capable of withstanding a voltage of 1200 V and a current 50 A. An isolator (MCT2E) is used to obtain the gate pulses. The five-level six-phase inverter has six-legs divided into two sets of three-legs with IGBT switches connected in parallel and supplied by a common DC-link (dSPACE DS1104). A real-time controller is used to generate the control pulses required to turn ON the main switches in the power circuit and these pulses are then fed to a gate drive circuit. As per the requirement of IGBTs, voltage +5 V is amplified to +15 V and −5 V. Open-loop volt/hertz control is used for controlling the drive. The proposed scheme was implemented in MATLAB/Simulink first and then interfaced with the real-time platform. The inverter requires multiple DC sources depending upon the number of primary cells cascaded. The current sensor (LEM LA 25-NP) was used with the voltage sensor (LV 10-1000) to measure the respective values of currents and voltages. All the waveforms were recorded using the power analyzer scope Yokogawa DL750, and the corresponding harmonics recorded using

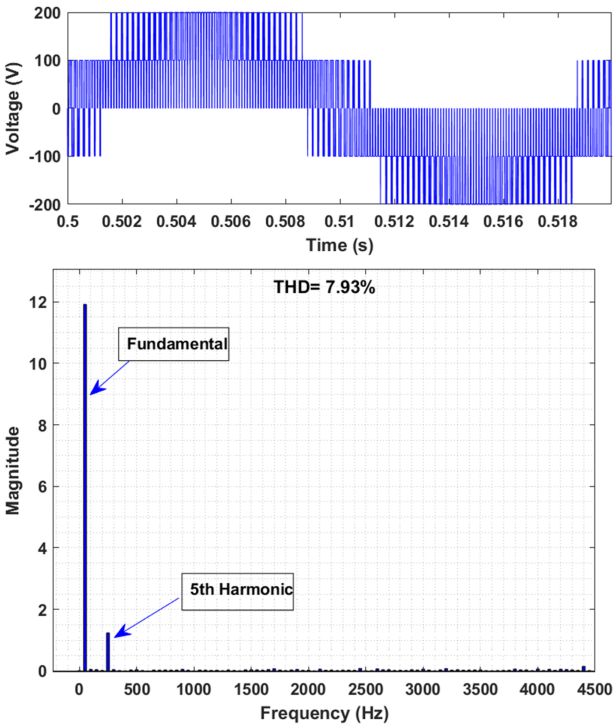

***Fig. 11**: Five-level stator phase voltage with fundamental and 5^{th} harmonic component.*

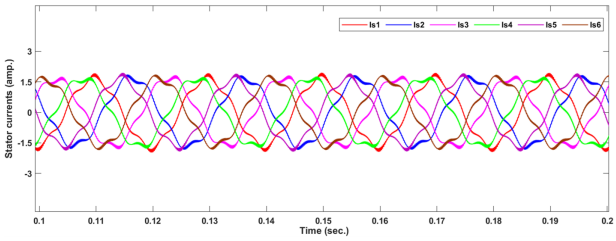

***Fig. 12**: Variation of stator currents in q_5-d_5 sub-space.*

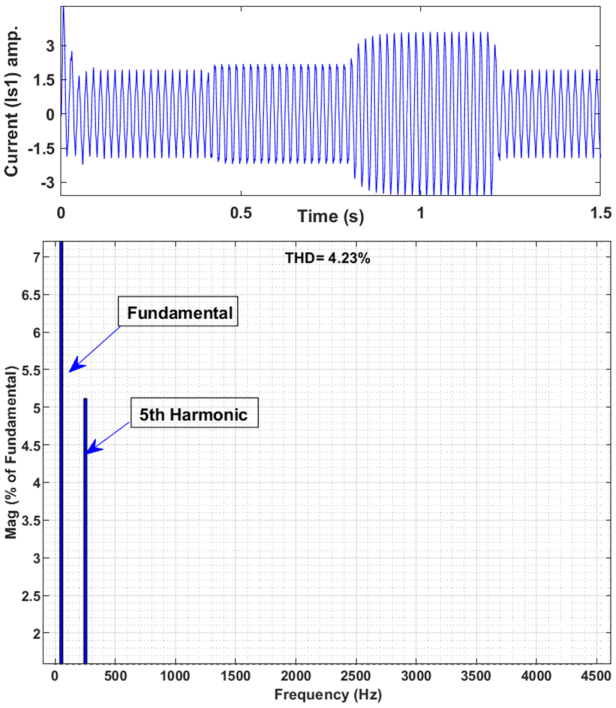

***Fig. 13**: Stator current I_{s1} with harmonic content in q_5-d_5 sub-space.*

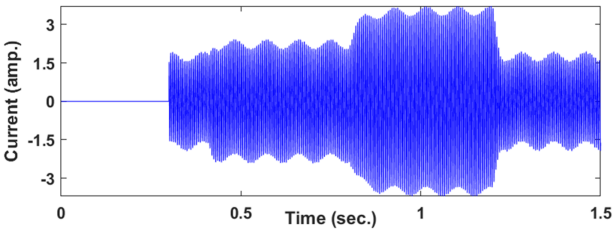

***Fig. 14**: Variation of stator currents I_{s1} and I_{s5} in q_5-d_5 sub-space.*

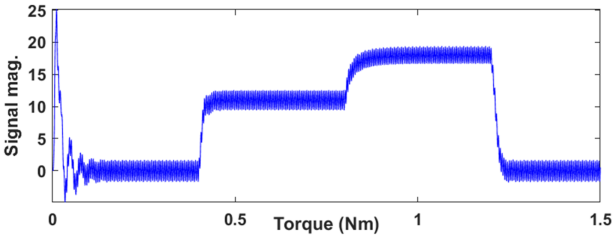

***Fig. 15**: Variation of motor torque under change of load conditions.*

the FLUKE power analyzer. The snapshot of the complete test rig is shown in Fig. 16.

Fig. 17 illustrates the six output voltages (V_{s1}, V_{s2}, V_{s3}, V_{s4}, V_{s5}, and V_{s6}) of the six-phase inverter using the proposed SVPWM technique for the fundamental component. The variation in six stator currents (I_{s1}, I_{s2}, I_{s3}, I_{s4}, I_{s5}, and I_{s6}) containing fundamental components under steady-state is illustrated in Fig. 18. The validation of the numerical simulation for the two cases is shown in Figs. 19–22.

For the balanced and sinusoidal supply as the input (Case I), the resultant five-level stator phase voltage with its harmonic content is shown in Fig. 19. The recorded waveform in Fig. 20 shows a stator current (I_{s1}) of 2.41 A flowing through the machine with a total harmonic distortion (THD) of 2.2%, which is approximately equal to the harmonic distortion of 2.23% obtained during the simulation.

For the fifth harmonic introduced into the reference voltage (Case II), the resultant five-level line-to-neutral stator phase voltage has fundamental and fifth harmonic components only (see Fig. 21). Also, the stator current (I_{s1}) under this case has a magnitude of 3.62 A and a harmonic distortion of 5.1%, as shown in Fig. 22, nearly following the THD of 4.23% obtained during the simulation test. Finally, Fig. 23 shows the variation in electrical torque (T_e) as a change in load torque (T_L), almost similar to the simulation result. Thus, from the analysis, it is clear that the simulation results are well corroborated by the experimental results, which, in turn,

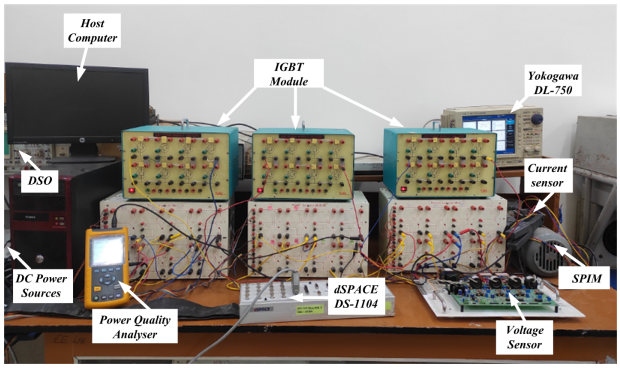

***Fig. 16**: General test rig.*

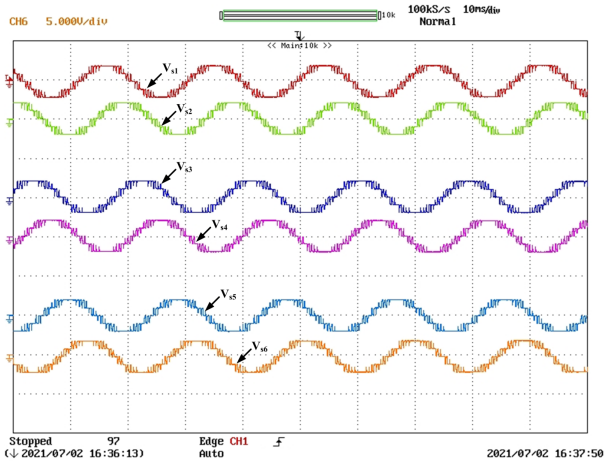

***Fig. 17**: Output voltages of the six-phase inverter.*

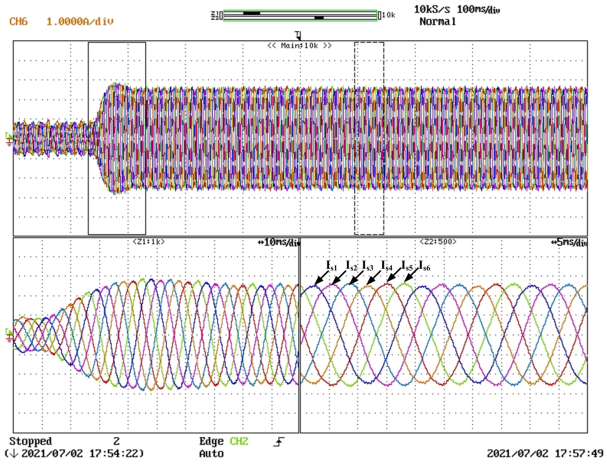

***Fig. 18**: Stator currents of the SPIM drive.*

verify the accuracy and efficacy of the proposed scheme.

Finally, a comparison between the conventional and proposed SVPWM inverter-based drives in terms of efficiency, power loss, and load torque is presented. The output frequency of the inverter is 50 Hz, and the sampling frequency is 5 kHz. Fig. 24 compares the THD performance of the conventional and proposed SVPWM drives. It is evident from the curve that the

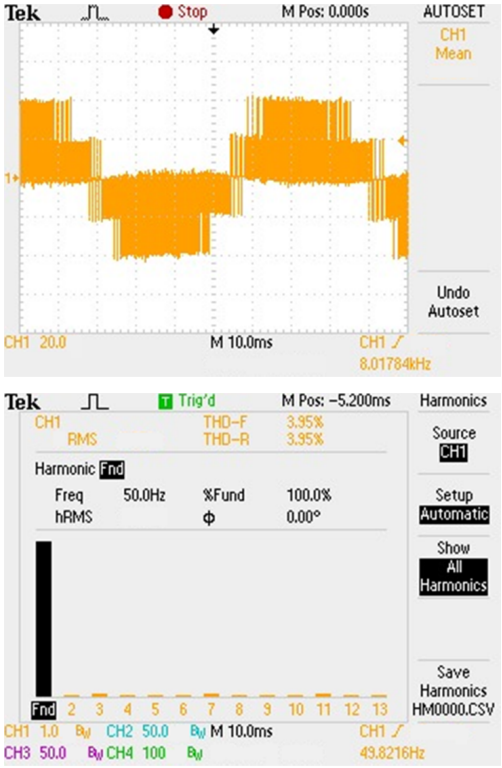

***Fig. 19**: Stator phase voltage with a fundamental component.*

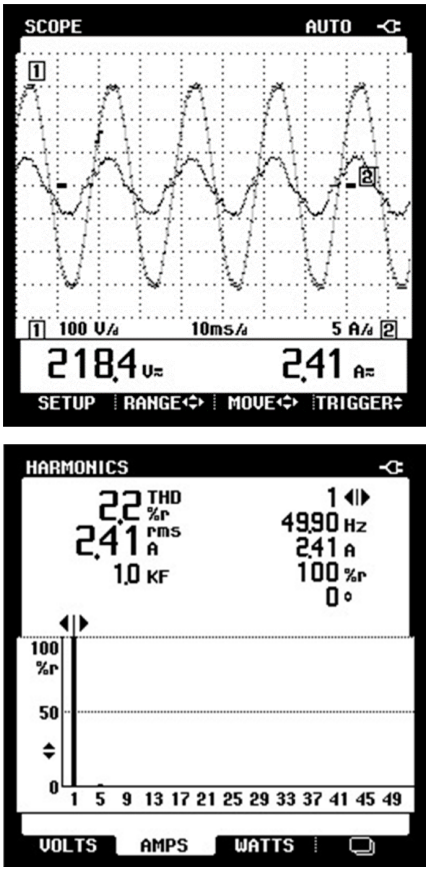

***Fig. 20**: Stator current I_{s1} with harmonic content (Case I).*

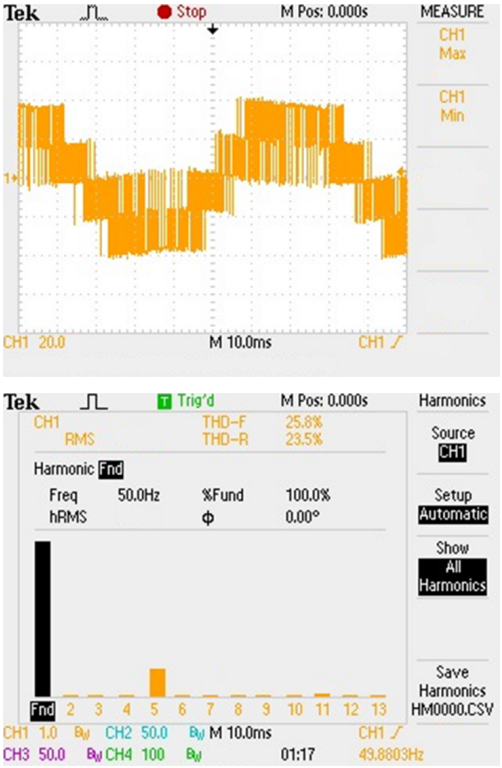

***Fig. 21**: Stator phase voltage with fundamental and 5^{th} harmonic component.*

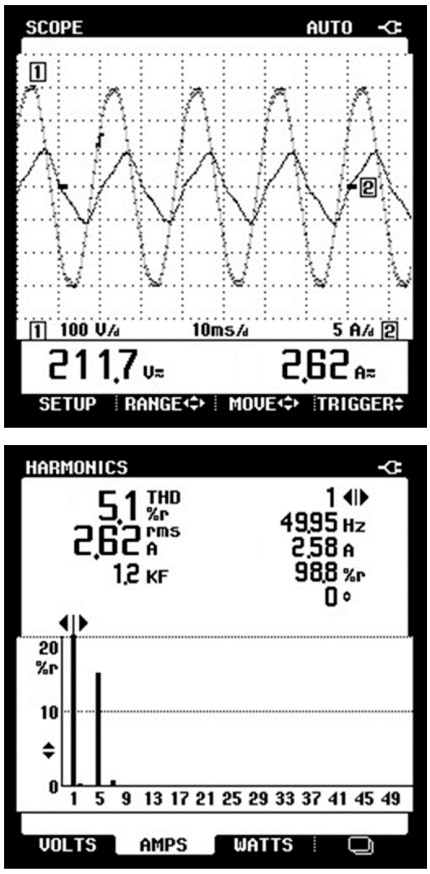

***Fig. 22**: Stator current I_{s1} with with harmonic content (Case II).*

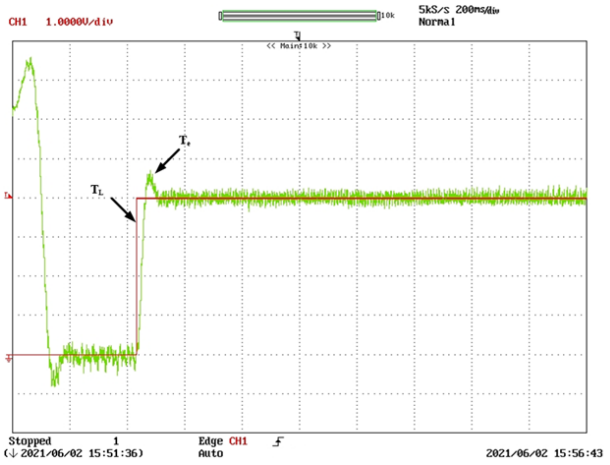

***Fig. 23**: Electrical torque (T_e) varies with load torque (T_L).*

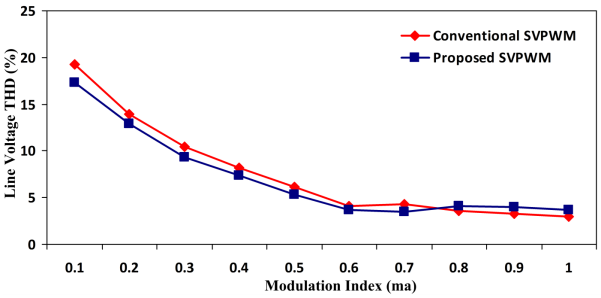

***Fig. 24**: THD performance of conventional and proposed SVPWM techniques.*

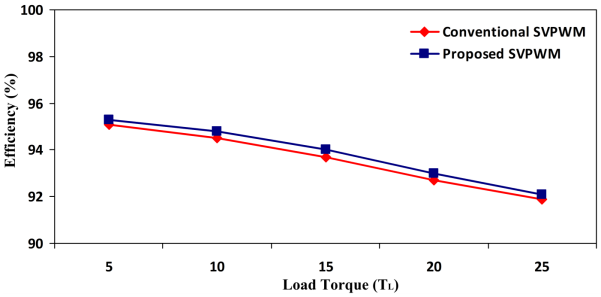

***Fig. 25**: Efficiency comparison between the conventional and proposed SVPWM techniques with change in load torque.*

proposed SVPWM offers lower THD at modulation index lower than 0.7 and slightly higher THD at modulation index higher than 0.8. Furthermore, the proposed technique reduces the calculation time and complexity of the space-vector control algorithm as compared to conventional SVPWM. Moreover, the proposed SVPWM has several advantages including well-defined switching operation, better utilization of DC-link voltage, and fast digital implementation.

From Fig. 25, it is evident that the proposed SVPWM drive's efficiency is slightly higher than the conventional SVPWM drive under different load torque operations. Table 2 compares the efficiency of the SPIM drive using

***Table 2**: Comparison between the conventional and proposed SVPWM techniques.*

Input	Power Loss (W)		Efficiency (%)	
Power (W)	Conventional	Proposed	Conventional	Proposed
225.9	19.1	18.8	91.9	92.0
293.1	23.6	22.6	92.7	93.0
329.9	27.1	25.8	93.7	94.0
392.7	29.8	27.7	94.5	94.9
430.2	32.8	32.1	95.1	95.2

the conventional and proposed SVPWM techniques. Switching and conduction losses represent the two main losses in the drives. The switching losses are determined when the device is turned ON or OFF, the total commutation time, and the current and voltages across the device during operation [14]. At the same time, the conduction losses are determined by the instantaneous current passing through the machine and the saturation voltage of the device. In this study, through simulation, input and output power are measured to estimate the efficiency, and the average current and saturation voltage of the device measured to estimate the conduction losses. The estimations show that conduction losses are higher than the switching losses. However, the conduction losses of the two techniques are almost equal, and thus, the efficiency of the drive by conventional and proposed SVPWM techniques are the same.

8. CONCLUSION

A modified SVPWM technique to drive a SPIM is presented in this paper. The proposed scheme provides for the independent multiple voltage control of two five-level, three-phase inverters in the *q-d* reference plane by optimally utilizing the input dc voltage. The modulation limit is determined under balanced and sinusoidal conditions. Comparative analysis between the conventional and proposed SVPWM reveals that a better performance can be achieved by implementing the proposed SVPWM inverter-based drive. Furthermore, experimental tests prove the mathematical developments and numerical analysis by taking a SPIM as the load. Finally, the closeness of the simulation and experimental results confirms the efficacy of the proposed scheme.

REFERENCES

[1] E. Levi, R. Bojoi, F. Profumo, H. Toliyat, and S. Williamson, "Multiphase induction motor drives – a technology status review," *IET Electric Power Applications*, vol. 1, no. 4, pp. 489–516, Jul. 2007.

[2] L. Parsa, "On advantages of multi-phase machines," in *31st Annual Conference of IEEE Industrial Electronics Society (IECON 2005)*, 2005, pp. 1574–1579.

[3] K. A. Chinmaya and G. K. Singh, "Experimental analysis of various space vector pulse width modulation (SVPWM) techniques for dual three-phase induction motor drive," *International Transactions on Electrical Energy Systems*, vol. 29, no. 1, Jan. 2019, Art. no. e2678.

[4] K. Mohapatra, R. Kanchan, M. Baiju, P. Tekwani, and K. Gopakumar, "Independent field-oriented control of two split-phase induction motors from a single six-phase inverter," *IEEE Transactions on Industrial Electronics*, vol. 52, no. 5, pp. 1372–1382, Oct. 2005.

[5] K. Marouani, L. Baghli, D. Hadiouche, A. Kheloui, and A. Rezzoug, "Discontinuous SVPWM techniques for double star induction motor drive control," in *32nd Annual Conference on IEEE Industrial Electronics (IECON 2006)*, 2006, pp. 902–907.

[6] V. Rathore and K. B. Yadav, "Direct torque control of asymmetrical multiphase (6-phase) induction motor using modified space vector modulation," in *Recent Advances in Power Electronics and Drives*, J. Kumar and P. Jena, Eds. Singapore: Springer, 2021, vol. 707, pp. 511–516.

[7] D. Hadiouche, L. Baghli, and A. Rezzoug, "Space-vector PWM techniques for dual three-phase AC machine: analysis, performance evaluation, and DSP implementation," *IEEE Transactions on Industry Applications*, vol. 42, no. 4, pp. 1112–1122, Jul. 2006.

[8] A. Bakhshai, G. Joos, and H. Jin, "Space vector PWM control of a split-phase induction machine using the vector classification technique," in *Thirteenth Annual Applied Power Electronics Conference and Exposition (APEC '98)*, vol. 2, 1998, pp. 802–808.

[9] P. Kumar, V. Rathore, and K. Yadav, "Fault tolerance study of symmetrical six-phase induction drive," in *2020 First IEEE International Conference on Measurement, Instrumentation, Control and Automation (ICMICA)*, 2020.

[10] D. Yazdani, S. A. Khajehoddin, A. Bakhshai, and G. Joos, "A generalized space vector classification technique for six-phase inverters," in *2007 IEEE Power Electronics Specialists Conference*, 2007, pp. 2020–2054.

[11] R. Bojoi, A. Tenconi, F. Profumo, G. Griva, and D. Martinello, "Complete analysis and comparative study of digital modulation techniques for dual three-phase AC motor drives," in *33rd Annual IEEE Power Electronics Specialists Conference*, 2002, pp. 851–857.

[12] E. Levi, "Advances in converter control and innovative exploitation of additional degrees of freedom for multiphase machines," *IEEE Transactions on Industrial Electronics*, vol. 63, no. 1, pp. 433–448, Jan. 2016.

[13] V. Rathore and K. B. Yadav, "Analytical model based performance characteristics analysis of six-phase induction motor," in *Proceedings of the International Conference on Advances in Electronics, Electrical & Computational Intelligence (ICAEEC 2019)*, 2019.

[14] E. Wiechmann, P. Aqueveque, R. Burgos, and J. Rodriguez, "On the efficiency of voltage source

and current source inverters for high-power drives," *IEEE Transactions on Industrial Electronics*, vol. 55, no. 4, pp. 1771–1782, Apr. 2008.

Vishal Rathore received his B.E. degree in Electrical and Electronics Engineering from Laxmi Narayan College of Technology (LNCT), Bhopal, India, in 2007, M.Tech in Electrical Drives from Maulana Azad National Institute of Technology (MANIT), Bhopal, India, in 2012. Currently, he is working towards his Ph.D. degree at National Institute of Technology (NIT) Jamshedpur, Jharkhand, India. His fields of interest include Multilevel Inverters based Multiphase Drives, Real-time controllers for power electronics based drives systems, and usage of power electronics in transit systems.

Krishna Bihari Yadav received his B.Sc. in Electrical Engineering from Regional Institute of Technology presently National Institute of Technology Jamshedpur, India, in 1989, M.Sc. in power electronics and Ph.D. from Indian Institute of Technology Roorkee, India, in 2007. Currently, he is an Associate Professor in the Department of Electrical Engineering at the National Institute of Technology Jamshedpur, India. His fields of interest include Multiphase electrical machines, Power Electronics & Electric Drives, Power System Economics, Renewable power generation.